miR-22 eluting cardiovascular stent based on a self-healable spongy coating inhibits in-stent restenosis

Jing Wang [a], Hong-Lin Qian [a], Sheng-Yu Chen [b], Wei-Pin Huang [a], Dan-Ni Huang [a], Hong-Ye Hao [a], Ke-Feng Ren [a,b,*], Yun-Bing Wang [c,**], Guo-Sheng Fu [b,***], Jian Ji [a,b]

[a] *MOE Key Laboratory of Macromolecular Synthesis and Functionalization, Department of Polymer Science and Engineering, Zhejiang University, Hangzhou, 310027, China*
[b] *Key Laboratory of Cardiovascular Intervention and Regenerative Medicine of Zhejiang Province, Department of Cardiology, Sir Run Run Shaw Hospital, Zhejiang University, Hangzhou, 310016, China*
[c] *National Engineering Research Center for Biomaterials, Sichuan University, Chengdu, 610064, China*

ARTICLE INFO

ABSTRACT

The in-stent restenosis (IRS) after the percutaneous coronary intervention contributes to the major treatment failure of stent implantation. MicroRNAs have been revealed as powerful gene medicine to regulate endothelial cells (EC) and smooth muscle cells (SMC) in response to vascular injury, providing a promising therapeutic candidate to inhibit IRS. However, the controllable loading and eluting of hydrophilic bioactive microRNAs pose a challenge to current lipophilic stent coatings. Here, we developed a microRNA eluting cardiovascular stent via the self-healing encapsulation process based on an amphipathic poly(ε-caprolactone)-poly(ethylene glycol)-poly (ε-caprolactone) (PCL-PEG-PCL, PCEC) triblock copolymer spongy network. The miR-22 was used as a model microRNA to regulate SMC. The dynamic porous coating realized the uniform and controllable loading of miR-22, reaching the highest dosage of 133 pmol cm^{-2}. We demonstrated that the sustained release of miR-22 dramatically enhanced the contractile phenotype of SMC without interfering with the proliferation of EC, thus leading to the EC dominating growth at an EC/SMC ratio of 5.4. More importantly, the PCEC@miR-22 coated stents showed reduced inflammation, low switching of SMC phenotype, and low secretion of extracellular matrix, which significantly inhibited IRS. This work provides a simple and robust coating platform for the delivery of microRNAs on cardiovascular stent, which may extend to other combination medical devices, and facilitate practical application of bioactive agents in clinics.

1. Introduction

Cardiovascular disease (CVD) is a leading cause of morbidity and mortality around the world [1]. Latest epidemiological studies in China have estimated about 320 million patients suffering from CVD, resulting in over 40% of CVD-related deaths against the total [2]. The percutaneous coronary intervention (PCI), particularly drug-eluting stent (DES) with controlled local release of anti-proliferative drugs, has become the gold standard in the treatment of coronary vascular diseases [3–5]. Despite the excellent outcomes, recent experimental and clinical trials have revealed severe complications after DESs implantation including late stent restenosis (LSR), neoatherosclerosis, and stent thrombosis (ST) [6–11]. In particular, clinical researches have reported that uncover struts and neoatherosclerosis are most frequently observed in late/very late ST. [12,13], indicating that the local release of anti-proliferative drugs delays the recovery of the endothelium [14,15]. Moreover, the incomplete recovery of endothelium could induce localized blood flow disturbance and further contribute to the formation of neo-atherosclerosis [16]. Therefore, it is highly desirable to develop the next generation of stent coatings with the capability of inhibiting intimal

hyperplasia without impairing the regeneration of the endothelium [17–19].

Micro-ribonucleic acids (miRNAs) are short (~22 nucleotides length) non-coding RNAs that bind to specific mRNA targets and regulate their translation and degradation [20]. Recent studies have revealed miRNAs as regulators that play a crucial role in the development of cardiovascular pathophysiologic processes [21,22]. Specifically, miRNAs have been substantially verified as gene regulators to induce vascular smooth muscle cell (VSMC) differentiation and phenotype switching in response to vascular diseases or injury [21,23]. For instance, miR-145 and miR-143 cooperatively target a network of transcription factors to regulate the quiescent versus proliferative phenotype of smooth muscle cells, which are downregulated after vascular injury [24]. The expression of miR-21 is enhanced in the atherosclerotic lesions or after vascular injury, leading to chronic hypoxia-induced vascular remodeling [25]. Meanwhile, it is well accepted that the phenotype switch of contractile VSMCs to proliferative synthetic cells plays a central role in the intimal hyperplasia after an intervention [26–28]. In this context, miRNAs offer a promising therapeutic target for specific inhibition of SMC proliferation and phenotype switching. Despite the enormous potential, the localized delivery of miRNAs based on stent implantation is still challenging: 1) the incorporation process should be gentle to avoid the impair to therapeutic effect; 2) controllable dosage and sustained release profile should be realized. Unfortunately, the preparation of current stent coatings mainly relies on the spraying of lipophilic polymers using organic solvents, which is unsuitable for the incorporation of water-soluble miRNAs. There remains an urgent need to develop an alternative coating method that can meet the requirement of miRNA delivery.

Microporous materials that enable wicking action provide an attractive way for bioactive agent incorporation [29–31]. The key feature of this capillarity-based wicking process is simple, gentle, and generally independent of the solute in the adsorbed solution [32,33], which would be favorable for the on-demand loading of bio-functional agents and fulfilling the "load-and-play" concept [34,35]. Herein, we report on a miRNA-eluting stent coating via the self-healing encapsulation process for suppression of SMC phenotype switching induced intimal hyperplasia (Scheme 1). The self-healable spongy coating was constructed based on an amphipathic poly(ε-caprolactone)-poly (ethylene glycol)-poly(ε-caprolactone) (PCL-PEG-PCL, PCEC) triblock copolymer network [34]. miR-22 was chosen as a target miRNA due to the effective mediation of SMC phenotype switching [36]. We firstly verified the controllable incorporation of miR-22 based on the wicking and healing process and tested the release profile of miR-22 after the healing process. Then, the effect of miR-22 eluting coating on the SMC phenotype switching, the competition growth of ECs versus SMCs, and

regulation on ECs were studied. Furthermore, the miR-22 eluting coating was prepared on the cardiovascular stent, and an *in vivo* experiment was performed using a porcine coronary artery injury model, in which the phenotype modulation and anti-restenosis performance were evaluated.

## 2. Experimental section

2.1. Materials

ε-Caprolactone (ε-CL), stannous octoate (Sn(Oct)$_2$), 4-methoxyphenol, 2-Hydroxy-4'-(2-hydroxyethoxy)-2-methylpropiophenone (I2959), Methacrylate anhydride (MAA), poly(ethylene glycol) (PEG, Mn = 2000), Polyvinylpyrrolidone (PVP, Mw = 10000) and gelatin (medium gel strength) were purchased from Sigma-Aldrich. 2-Isocynatoethyl methacrylate (IEM) was obtained from Aladdin (Shanghai, China). ssc-miR-22-3p mimic (mature miRNA sequence: AAGCUGCCAGUUGAA-GAACUGU), cy3-labeled ssc-miR-22-3p mimic, and miR-ctrl (mature miRNA sequence: UUUGUACUACACAAAAGUACUG) were purchased from Guangzhou RiboBio Co., Ltd. PBS was purchased from Sango Biotech (Shanghai, China). Qubit™ microRNA Assay Kit, CellTracker™ Green CMFDA Dye, and CellTracker™ Red CMTPX Dye were obtained from ThermoFisher Scientific Co., Ltd. FITC-labeled bovine serum albumin (BSA) was obtained from ZhongKeChenYu biotech (Beijing, China). The deionized (DI) water (>18 MΩ cm) used in all experiments was purified with a Millipore Milli-Q water purification system. All materials were used as received without further purification.

2.2. Construction of the self-healable spongy coatings

The PCL-PEG-PCL diacrylate (PCECDA25) triblock copolymer was synthesized as our previous work [34]. For the preparation of PCEC spongy coating, PCECDA, PVP, and I2959 were dissolved in CH$_2$Cl$_2$ with a mass ratio of 200:50:1, respectively. The initial coating was sprayed on a substrate using an ultrasonic spray system (Ruidu Photoelectric Technology Co. Ltd, Shanghai), followed by UV photo-crosslinking process for 5 min (Intelli-Ray 400, USA). The microporous structure was obtained by immersion into DI water at 45 °C for a given time, followed by freeze-drying process. Scanning electron microscopy (SEM, Hitachi S4800, Japan) was performed to observe the microstructure formation within the PCEC coating. ATR-FIIR was used to verify the removal of PVP.

2.3. Loading and releasing of miR-22

The PCEC spongy coating (12 mm in diameter) was first treated with
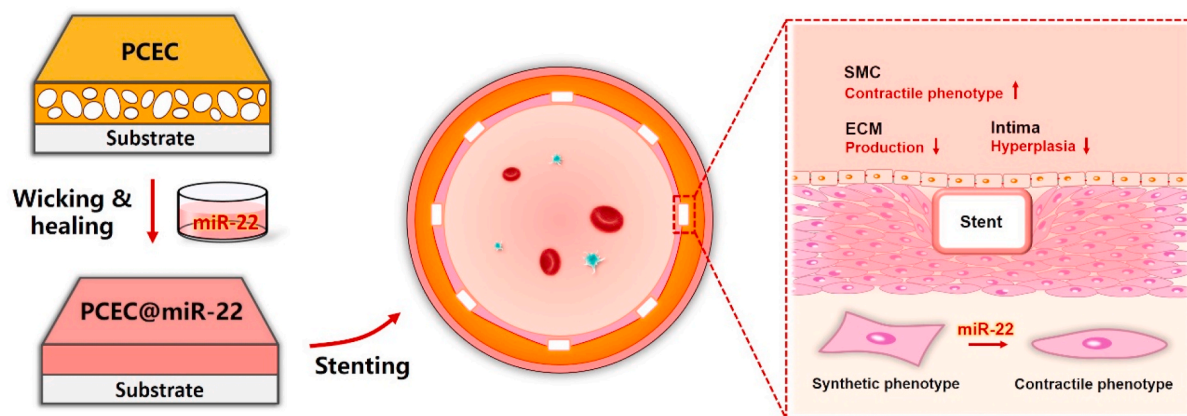
Scheme 1. Schematic illustration of the preparation of the PCEC@miR-22 coated stent. The miR-22 was loaded into PCEC spongy coating based on a wicking action and subsequent self-healing encapsulation.

20 µL of miR-22 solution for the wicking action. After 5 min incubation, the PCEC spongy film was heated up to 45 °C to heal the internal pores, followed by rinsing with 200 µL DI water 3 times. The miRNA content in the wicking solution and the rinsing solution was measured by Qubit™ microRNA Assay Kit. The miRNA dosage was determined by the subtraction of miRNA in wicking solution and collected rinsing solution. All samples were kept under vacuum at room temperature for 24 h to remove the residual water. Cy3 labeled miR-22 was used to determine the distribution of miR-22 within the PCEC coatings via a Laser Scanning Confocal Microscope (FV3000-OSR, Olympus, Japan).

The release behavior of miR-22 was performed in TE buffer (pH 7.4, 37 °C) in Eppendorf DNA LoBind tubes. The TE buffer was frequently replaced at appropriate time points to ensure constant release conditions. The miR-22 content in the extraction solution was measured by Qubit™ microRNA Assay Kit.

2.4. Blood compatibility analysis

For the platelet adhesion test, samples were incubated with platelet-rich plasma for 2 h at 37 °C, washed gently with PBS 3 times, and fixed with 2.5% glutaraldehyde for 30 min. After dehydration by graded ethanol (20%, 40%, 50%, 60%, 70%, 80%, 90%, 100%), all samples were observed by SEM (Hitachi S4800, Japan).

Different samples were incubated with platelet-poor plasma and activated partial thromboplastin time/thrombin time (APTT/TT) reagents (Jiancheng Bioengineering, China) successively. Plasma clotting time was recorded. Whole blood clotting time (WBCT) tests were performed on different samples for given times (5, 10, and 15 min). Histograms of digital photos were analyzed using ImageJ software (NIH, Bethesda, MD, USA).

2.5. Smooth muscle cell culture and evaluation

Methacrylic anhydride (MAA) modified gelatin (MeGel, obtained according to previous work [37–39]) was used to promote cell adhesion in cell culture evaluation. In brief, the PCEC spongy coating was treated with 20 µL wicking solution containing miR-22 (in desired concentration), MeGel (10 mg/mL) and I2959 (0.5 mg/mL). After 5 min wicking action, the PCEC coating was heated up to 45 °C for the healing process, followed by 5 min UV treatment for gelatin modification. All samples were rinsed by PBS, blown dry, and kept at low temperature before use.

For the proliferation test, SMCs were firstly stained by CellTracker™ Green CMFDA Dye, then seeded onto different samples in 24-well culture plates at a density of 20 000 cells per cm^2. After incubation for 48 h, all samples were fixed by 4% paraformaldehyde, stained with nuclei (1:100, DAPI, Sigma), and mounted onto clean coverslips with the antifade reagent. At least 5 fluorescence micrographs were taken for the cell proliferation test (DS-Ri2, Nikon, Japan). MTT test was also adopted to quantitively evaluate cell proliferation.

The regulation of miR-22 on SMCs was evaluated via immunofluorescence analysis and relative mRNA level analysis. SMCs were seeded on different samples at a concentration of 20 000 cells per cm^2. After 3 d culture, all samples were gently washed with PBS, fixed with 4% paraformaldehyde, and treated with 0.1% Triton X-100. Cell staining was performed for nuclei (1:100, DAPI, Sigma) and calponin (1:300, monoclonal anti-calponin antibody, sigma), and observed by fluorescence microscopy (DS-Ri2, Nikon, Japan). The expression of ecotropic virus integration site 1 protein homolog (EVI-1), α-smooth muscle actin (α-SMA), methyl-CpG binding protein 2 (MECP2), and collagen-I (Col-I) was analyzed by real-time quantitative PCR (RT-qPCR) assay (CFX384, BioRad, Hercules, CA, USA). SMCs on different samples were lysed for RNA extraction by TRIzol reagent (Haogene Biotech, Shanghai, China). The primer sequences for tested genes were shown in supporting information.

2.6. Endothelial cell culture and evaluation

For the proliferation test, HUVECs (Human umbilical vein endothelial cells) were firstly stained by CellTracker™ Red CMTPX Dye, then seeded onto different samples in 24-well culture plates at a density of 20 000 cells per cm^2. After incubation for 48 h, all samples were fixed by 4% paraformaldehyde, stained with nuclei (1:100, DAPI, Sigma), and sealed with the antifade reagent. At least 5 fluorescence micrographs were taken for the cell proliferation test (DS-Ri2, Nikon, Japan). MTT test was also adopted to quantitively evaluate cell proliferation.

The effect of miR-22 on ECs was evaluated as follows: ECs were seeded on different samples at a concentration of 20 000 cells per cm^2. After 3 d culture, all samples were gently washed with PBS, fixed with 4% paraformaldehyde, and treated with 0.1% Triton X-100. Cell staining was performed for nuclei (1:100, DAPI, Sigma), von Willebrand factor (anti-vWF-red, Invitrogen) and CD31 (anti-CD31, Sigma). All samples were fixed onto clean coverslips with the antifade reagent and observed by fluorescence microscopy (DS-Ri2, Nikon, Japan). The expression of platelet endothelial cell adhesion molecule-1 (PECAM-1/CD31), VE-cadherin/CD144, and endothelial nitric oxide synthase (eNOS) were analyzed by real-time quantitative PCR (RT-qPCR) assay (CFX384, BioRad, Hercules, CA, USA). ECs on different samples were lysed for RNA extraction by TRIzol reagent (Haogene Biotech, Shanghai, China).

2.7. Co-culture

ECs and SMCs were stained using CellTracker™ Red CMTPX Dye and CellTracker™ Green CMFDA Dye respectively, then seeded on different samples at a density of 10 000 cells per cm^2 (total 20000 cells per cm^2). After coculture, all samples were fixed by 4% paraformaldehyde, stained with nuclei (1:100, DAPI, Sigma), and sealed with the antifade reagent. At least 5 fluorescence micrographs were taken to determine the cell density (DS-Ri2, Nikon, Japan).

2.8. Stent implantation and stent segments analysis

Biodegradable bare stents (3 mm in diameter, 13 mm in length) based on PLLA were provide by Xing Tai Pu Le biomedical technology Co., Ltd. PCEC spongy coating was constructed onto the stent. The mechanical properties of the stents were tested by a TRR2 radial force tester (Blockwise, USA). Bare stents were used as control. The loading of cy3 labeled miR22 was performed via wicking in 100 µL of miR-22 solution (25 µM) for 10 min, followed by the self-healing and rinsing process. The total dosage of miR-22 on stent was about 220 pmol per stent. SEM and confocal imaging were adopted to evaluate the miR-22 distribution on the stent. All of the animal experiments were performed by the Gateway Medical Innovation Center in Shanghai. Six white minipigs (25–35 Kg) with a total of 12 stents were used in this study following the guidelines of the Chinese Animal Care and Use Committee standards. The pig coronary artery was injured by balloon dilatation during the stent implantation process. The pressure applied for balloon dilatation was kept at the same level (8–10 bar) to ensure a similar injury level. Two evaluation stages with different time points (7 d and 28 d) were performed with 3 bare stents and 3 miR-22 eluting stents for each stage group. It was ensured that no branches were presented in the stented region. Digital angiography was recorded before and after implantation. All animals were treated with gentamicin sulfate (5 mg/kg) by intramuscular injection in the next three days and fed with a normal diet containing 150 mg aspirin and 300 mg clopidogrel every day.

Pigs were euthanized at 7 d and 28 d. The stented artery samples with implantation for 7 d were excised and washed quickly with saline, followed by freezing in liquid nitrogen. Half of the samples were used for RT-qPCR analysis to evaluate the mRNA level of EVI-1 and MECP2 (The primer sequences were shown in supporting information). The rest of the frozen samples were homogenized in RIPA lysis buffer with protease

inhibitors. Western blot assay was applied to evaluate the expression of Col-I, IL-6, MCP-1, and EVI-1, respectively. The health arteries without stent implantation were adopted as control.

The stented artery samples with implantation for 28 d were excised and fixed in 5% phosphate-buffered formalin for 24 h. Then, samples were embedded in paraffin for cross-section slicing (3 representative sections for each artery segment). Seven slices were prepared at each section, two of which were performed by hematoxylin-eosin (HE) and Masson staining for the histological analysis of the neointimal hyperplasia [9,40]. Three slides were processed for immunohistochemistry of α-smooth muscle actin (α-SMA), calponin-1 (CNN1), and collagen-I (Col-I), respectively. One slide was used for immunofluorescence evaluation of calponin-1 (CNN1). The last slide was used for the detection of cy3 labeled miR22. Representative micrographs were taken by an optical microscope (DS-Ri2, Nikon, Japan).

2.9. Statistical analysis

All data were obtained from at least three independent experiments with at least three parallel samples per condition in each experiment and expressed as mean ± standard deviation (SD). Statistical significance was assessed with Student's t-test, and a probability value of $p < 0.05$ is considered as statistically significant.

3. Results and discussion

3.1. Preparation of PCEC healable spongy coating

The PCEC amphipathic copolymer was synthesized and confirmed via ^{1}H-NMR (Fig. S1, supporting information) according to our previous work [34]. The PCEC spongy coating was prepared by swelling and freeze-drying process (Fig. 1a), and we selected PVP doping to enhance the water-uptake ability during the spraying step. Fig. 1b shows the

evolution of the microstructure on the top surface and within the internal section as a function of swelling time. The PCEC coating showed porous microstructures with large pores on the top-region and small pores within the down-region after 5 min swelling treatment, indicating that the doped PVP dramatically accelerated the water-uptake process that previously required over 30 min [34]. The average pore volume of PCEC coating increased from 22% to 42% when the swelling process prolonged from 5 min to 40 min (Fig. 1c), and the pore density of the PCEC coating increased from 7.1×10^4 to 1.73×10^5 per mm^2, simultaneously. The internal pore size of the PCEC coating also increased with the prolonged swelling while the pore size on the top-region remained the same level, which could be attributed to the increase of water content. The abundant and evenly distributed micropores on the top surfaces could benefit the fast loading of functional agents, while the large and interconnected porous structure within the coating could be favorable for the diffusion of agents during wicking action [30,41]. Besides, the swelling process realized a desirable removal of PVP polymer (Fig. S2, supporting information). Therefore, we chose a 40 min swelling process for the construction of the PCEC spongy coating in the following experiments.

3.2. miR-22 loading and release behavior

We employed a self-healing encapsulation method for the loading of miR-22 as illustrated in Fig. 2a. The self-healing ability of PCEC spongy coating was firstly studied by heating up to 45 °C, and the development of the coating appearance and the corresponding microstructure is shown in Fig. 2b. The white opaque PCEC spongy coating gradually turned to a colorless transparent one in less than 1 min (Video S1, Supporting information). Correspondingly, the SEM micrographs confirmed the healing of micropores within the coating, indicating the rapid self-healing property of PCEC spongy coating. This thermo-triggered closure of the microporous structure was attributed to
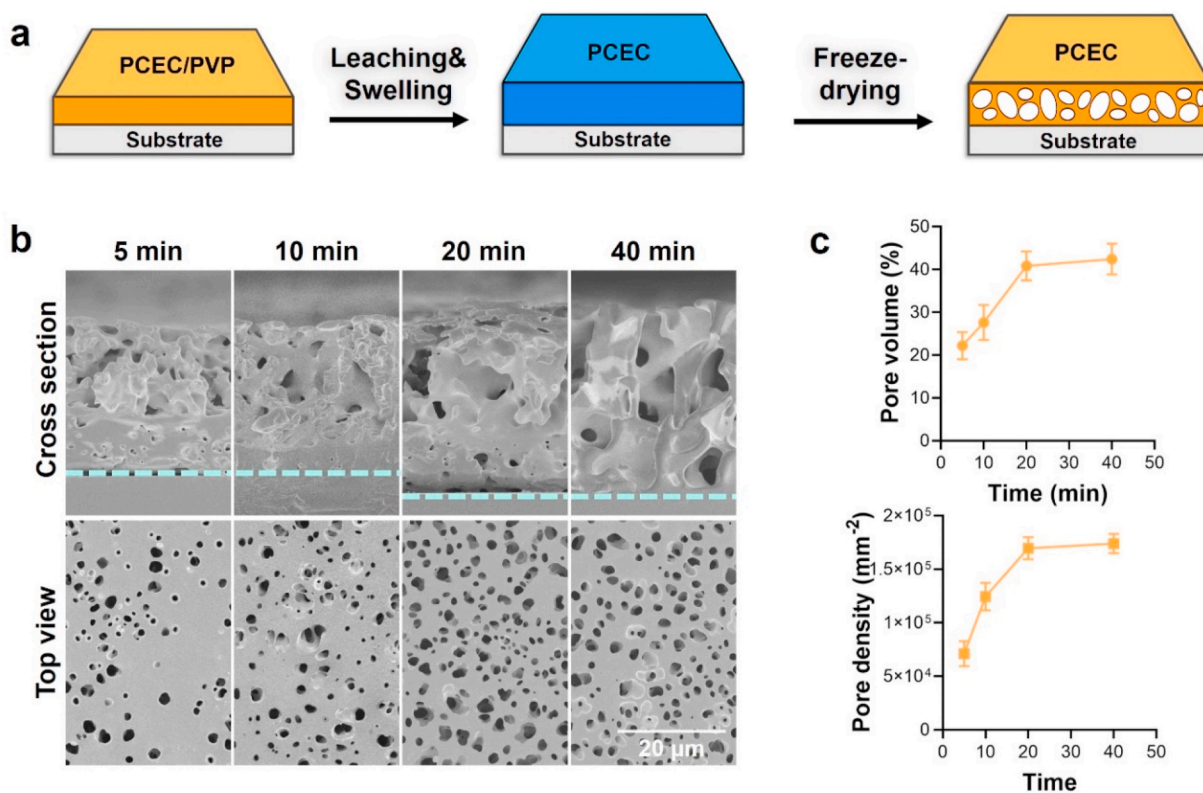
Fig. 1. Preparation of the PCEC microporous coating. (a) Illustration of the swelling and freeze-drying process. (b) SEM micrographs of the PCEC coating with different swelling times. (c) The pore volume and pore density of the PCEC coating with different swelling times.
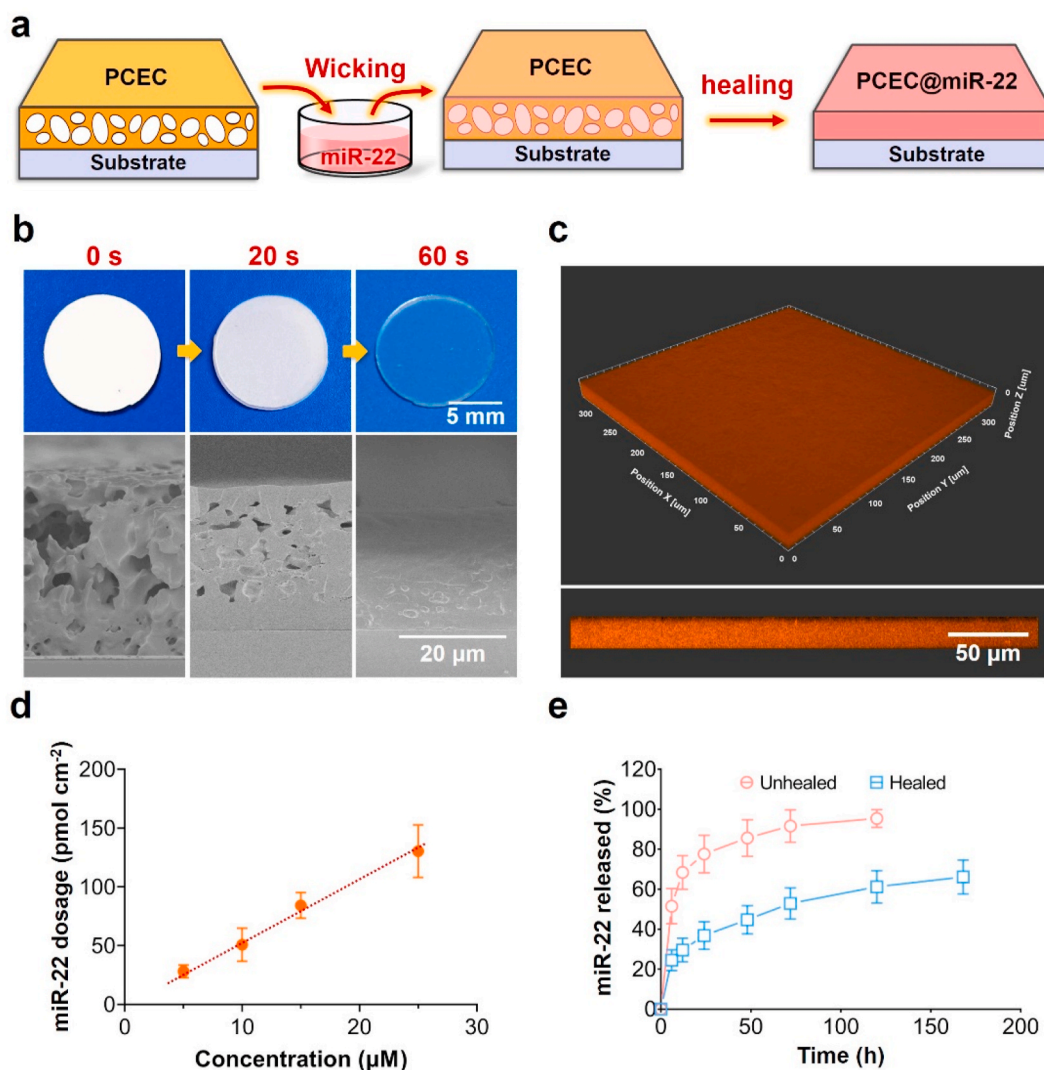
Fig. 2. The loading of miR-22 based on self-healing encapsulation. (a) Illustration of the loading process. (b) The digital photos and cross-sectional SEM micrographs of PCEC coating with different healing times. (c) The confocal micrographs of cy3 labeled PCEC coating. (d) The miR-22 dosage of PCEC coating as a function of wicking solution concentration. (e) The release behavior of PCEC@miR-22 coating before and after the healing process.

polymer-chain interdiffusion driven by minimization of energetically unfavorable interfacial area [42]. Next, we tested the loading ability of our PCEC coating using cy3 labeled miR-22. As shown in Fig. 2c, the orange fluorescence signal was uniformly distributed within the coating, suggesting a uniform encapsulation of miR-22. As a coating method for microRNA delivery, our self-healing encapsulation method realized a relatively uniform loading of functional agents that was feasible for practical applications.

Since the physiological functions of microRNA are dosage dependent [21–23], the dosage controllability of PCEC spongy coating was evaluated by wicking in various concentrations of miR-22. As shown in Fig. 2d, the total miR-22 dosage was 28.1 ± 4.5, 53.2 ± 8.9, 84.2 ± 8.9, and 133.1 ± 15.1 pmol cm^{-2} when the concentration of wicking solution was 5, 10, 15, and 25 μM, respectively. The loading dosage of miR-22 showed a linear relationship with the solution concentration, indicating the reliability of our method for tailoring the surface functionality. This controllable loading capacity is highly favorable for precision medicine that requires customized treatment [43,44]. Notably, the loading ratio of miR-22 in PCEC coating reached up to 27% when the wicking concentration was 25 μM, suggesting a high loading efficiency. Next, we evaluated the effect of healing process on the release profile of miR-22. During the initial 24 h, the PCEC coating before and after

healing process both showed a burst release of miR-22 with a cumulative release of $77.6 \pm 9.6\%$ and $36.8 \pm 6.9\%$, respectively. At 5 d, the cumulative miR-22 release was $95.4 \pm 4.4\%$ and $61.2 \pm 8.1\%$, respectively. The healing process of PCEC coating dramatically enhanced the retention of miR-22 due to the closure of porous structure and the formation of the crystalline region [34]. The healed PCEC coating exhibited a sustained miR-22 release profile that was in the range of previous studies for the delivery of genes and antibodies [45–48]. Besides, the PCEC coating before and after miR-22 loading both showed desirable blood compatibility property (Fig. S3, supporting information).

3.3. Regulation of ECs and SMCs on the miR-22 loaded coating in vitro

We evaluated the effect of miR-22 dosage on the cell proliferation properties of ECs and SMCs. As shown in Fig. 3a, the PCEC coating without miR-22 loading provided a similar cell adhesion to both ECs and SMCs. The encapsulation of miR-22 showed no significant influence on the proliferation of ECs when the dosage was below 133.1 pmol cm^{-2}. In contrast, the growth behavior of SMCs was remarkably depressed since the dosage was above 53.2 pmol cm^{-2}, indicating that SMCs were more sensitive to miR-22. Correspondingly, the calculated cell density of ECs became significantly higher than that of SMCs when the miR-22 dosage
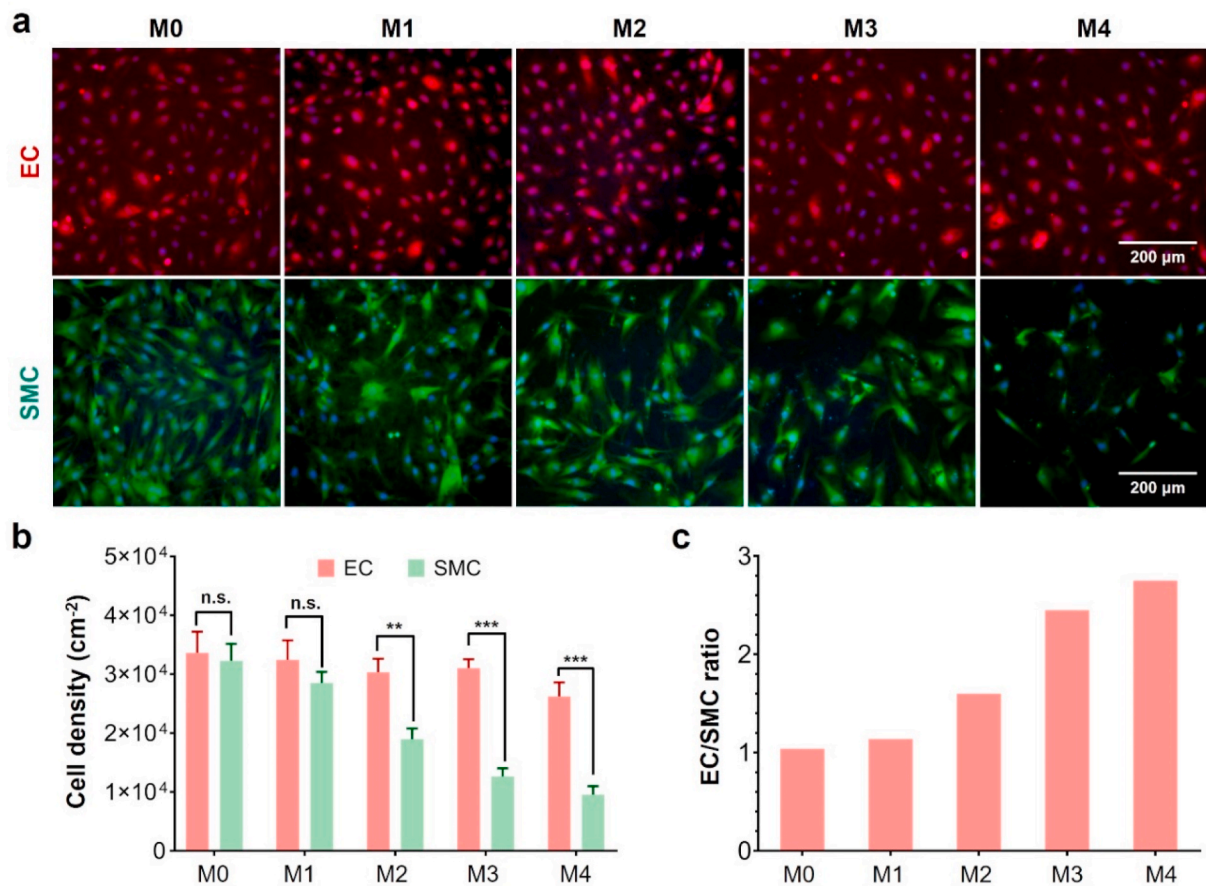
Fig. 3. The cell proliferation of EC and SMC on different PCEC@miR22 coating (M0, M1, M2, M3, M4 represents the miR-22 dosage of 0, 28.1 ± 4.5, 53.2 ± 8.9, 84.2 ± 8.9, and 133.1 ± 15.1 pmol cm^{-2}, respectively). (a) Fluorescence micrographs of EC (red) and SMC (green) on PCEC@miR-22 coating; (b) Cell density of EC and SMC; (c) The EC/SMC ratio on PCEC@miR-22 coating. (n = 5, **p < 0.01, ***p < 0.001).

was above 53.2 pmol cm^{-2} (Fig. 3b). Meanwhile, the cell density ratio of ECs/SMCs was about 1.6, 2.4, and 2.8 when the miR-22 dosage was 53.2, 84.2, and 133.1 pmol cm^{-2}, respectively. The MTT assay also showed a similar cell growth behavior (Fig. S4, supporting information). To selectively inhibit the growth of SMCs without impairing ECs, we therefore choose a miR-22 dosage of 84.2 pmol cm^{-2} for the following study.

Many studies have verified that miR-22 is related to a variety of cardiac diseases [49,50]. In particular, miR-22 plays a regulative role in the SMC phenotype switching and vascular neointima lesion formation via its target genes, MECP2, HDAC4, and EVI-1 [36]. To verify the regulation effect on the SMC phenotype, we selected the expression of calponin as a representative contractile phenotype marker during the SMC culture. As shown in Fig. 4a, the red fluorescence signal was dramatically enhanced when the SMCs were seeded on the miR-22 loaded PCEC coating, suggesting the promotion of contractile
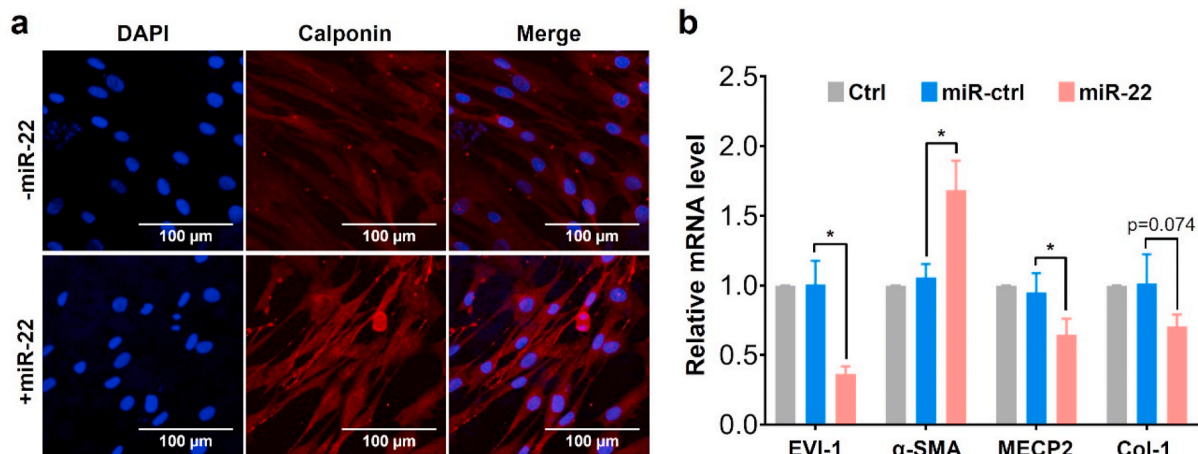
Fig. 4. The regulation of PCEC@miR-22 coating on the SMC phenotype: (a) Confocal micrographs of SMC. (blue: DAPI, red: Calponin); (b) The relative mRNA level of SMCs on different samples. (n = 3, *p < 0.05).

phenotype of SMCs. Moreover, the remarkable downregulation of EVI-1 and MECP2 (Fig. 4b) indicated that this self-healing encapsulation of PCEC spongy coating effectively preserved the bioactivity of miR-22 [36]. The dramatic increase of α-SMA on miR-22 loading samples suggested the improvement of the contractile phenotype of SMCs [51]. We also observed the down-regulative trend of the Col-I mRNA level, suggesting that miR-22 inhibited the extracellular matrix secretion. Many studies have revealed that the SMC phenotype switching from contractile to synthetic phenotype results in the migration, proliferation, and extracellular matrix (ECM) over-secretion of SMCs, which eventually contributes to the intimal hyperplasia [16,52,53]. Furthermore, SMC can adopt alternative phenotypes including resembling foam cells, macrophages, mesenchymal stem cells, and osteochondrogenic cells, which could contribute both positively and negatively to disease progression [54,55]. We verified that the miR-22 eluting coating in this study showed promotion of the SMC contractile phenotype, offering a positive regulation for vascular remodeling. Besides, the impact of miR-22 on EC functionality was also studied (Fig. S5, supporting information). The immunofluorescence evaluation on EC function-related marker vWF and CD31 showed no significant difference after the loading of miR-22. Meanwhile, the mRNA level of endothelium function-related genes, including CD31, CD144, and eNOS [56–58], also showed no significance after miR-22 loading. Collectively, our results indicated that the miR-22 loaded PCEC coating at a density of ~84.2 pmol cm^{-2} provided a microenvironment that dramatically promoted the contractile phenotype of SMC without impairing the growth of ECs.

3.4. Coculture of ECs with SMCs in vitro

Since the EC/SMC competitive growth behavior in coculture has been demonstrated to be more informative [9,18], we next evaluated the EC/SMC coculture behavior on the miR-22 loaded coatings. As shown in Fig. 5a, the ECs and SMCs cultured on TCPS and miR-ctrl (scrambled microRNA) samples showed a similar growth behavior. In contrast, the miR-22 loaded coating significantly depressed the proliferation of SMCs, which resulted in the dominating growth of ECs. The cell density calculation in Fig. 5b showed similar trends. After 4 d culture, the miR-22 loaded coatings realized a higher EC density to 5.4×10^4 per cm^2 and a more remarkable EC/SMC ratio of 5.4 as compared to miR-ctrl loaded coatings. Therefore, our results indicated that the miR-22 loaded PCEC coating realized the competitive growth of ECs over SMCs, which was beneficial for the regeneration of pure endothelium on stents [40, 59].
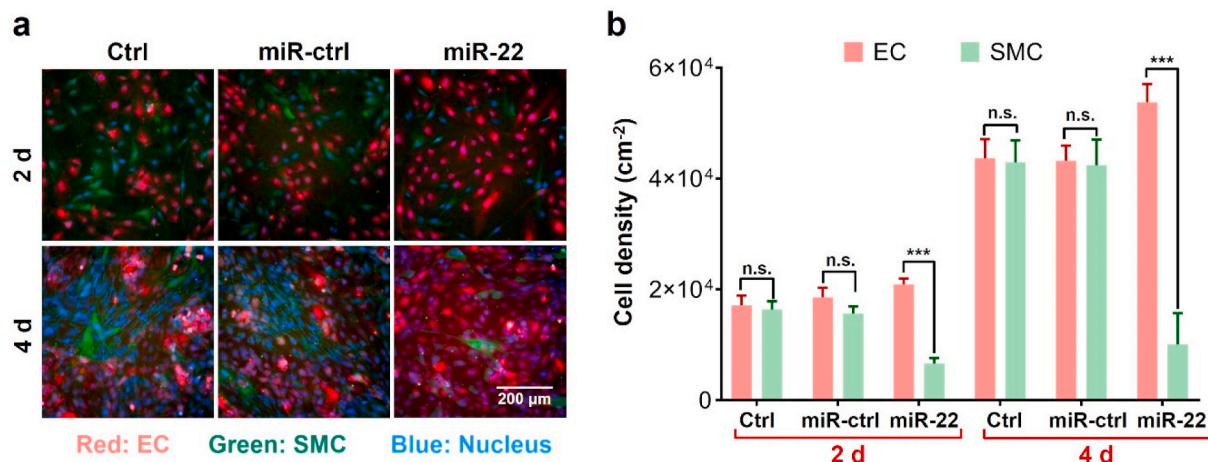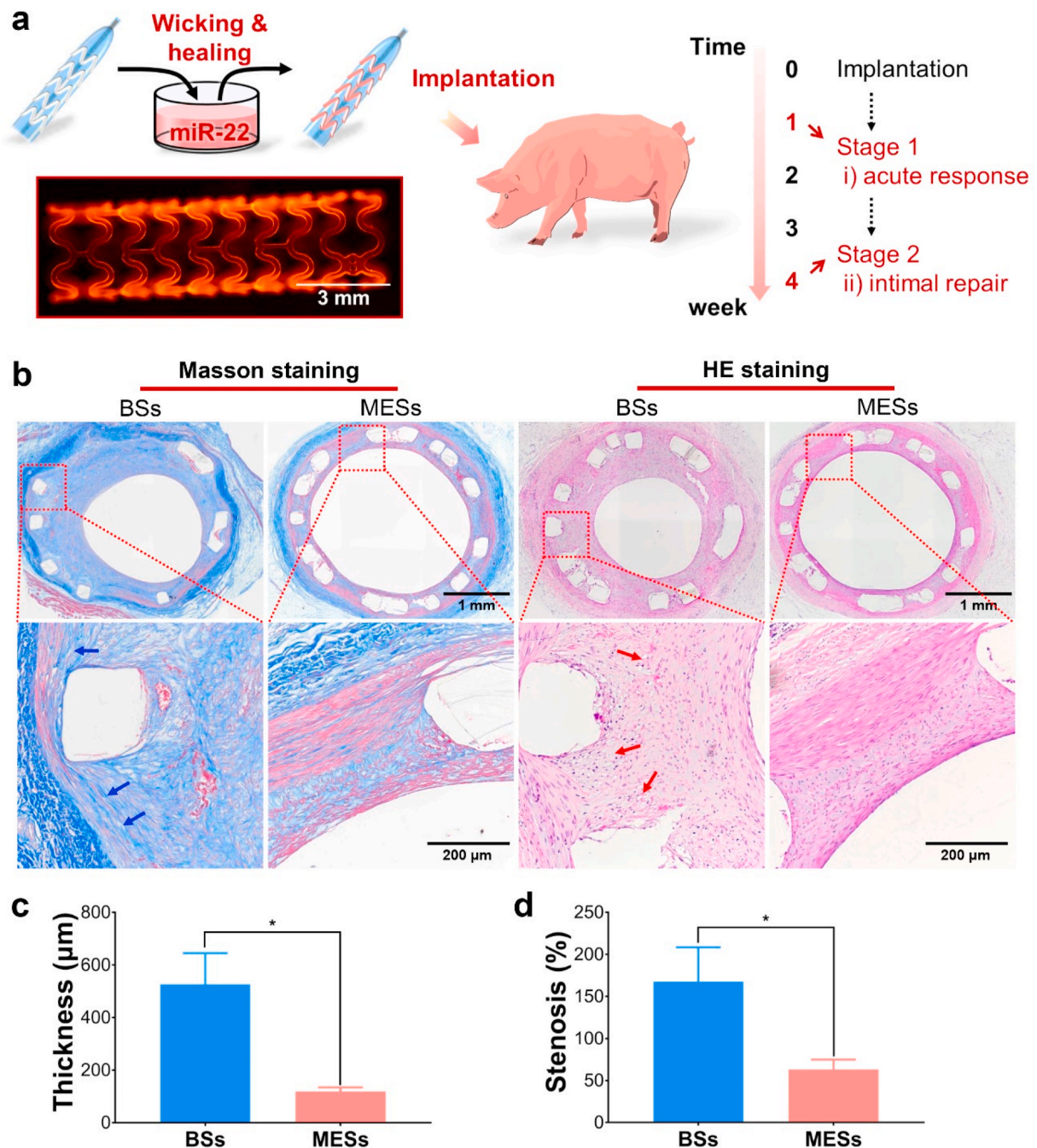
3.5. In vivo evaluation of miR-22 loaded PCEC coating on stents

To further verify the ability of PCEC@miR-22 coating for the inhibition of restenosis, we performed the *in vivo* stent implantation tests using a porcine coronary artery injury model. The preparation of miR-22 eluting stents (MESs) was illustrated in Fig. 6a. The PCEC coated stent after the healing process showed a smooth morphology and a uniform distribution of miR-22 on the stent (Figs. S6a–c, supporting information). Besides, the PCEC@miR-22 coating showed a negligible effect on the mechanical properties of the stents (Fig. S6d&e, supporting information). After the stent implantation, we observed a significant enhancement of the collagen expression and the presence of foamy areas in the BSs stented arteries (Fig. 6b), indicating the extensive proliferation of SMCs and the inflammation response caused by the artery injury [54]. Moreover, the Masson staining and HE staining analysis demonstrated that MESs with the miR-22 delivery dramatically reduced the intima hyperplasia as compared to bare stents (BSs) after 28 days implantation, the average neointimal thickness in MESs group was reduced by 77.5% as compared to BSs group (Fig. 6c). Meanwhile, the neointimal stenosis rate of MESs group was 62% lower than that of BSs (Fig. 6d). We also observed the significant distribution of miR-22 in the stented location (Fig. S7, supporting information). These results suggested that the self-healing encapsulation of our PCEC spongy coating platform effectively realized the localized delivery of miR-22, thus significantly suppressed the intimal hyperplasia after implantation.

To verified the function of our PCEC@miR-22 coating for phenotype regulation of SMCs, immunohistochemical staining for α-SMA and Col-I was performed (Fig. 7a&b). Compared to the BSs group, the MESs group showed significant promotion on the expression of α-SMA, verifying the remarkable enhancement of the contractile phenotype of SMCs [60,61]. We also observed a significant increasement in the CNN1 expression in the MESs group, which was consistent with the α-SMA expression evaluation (Fig. S8, supporting information). In addition, the secretion of Col-I in MESs group was much lower than that of the control group. It is well accepted that Col-I is the major component of the ECM structure generated from SMCs and fibroblasts [26]. The stent implantation caused the injury to the intima, which activated the SMC phenotype switching and thus promoted the extensive secretion of Col-I, eventually contributing to the neointimal hyperplasia [16,26]. In this work, we realized the miR-22 delivery via a self-healing encapsulation method, which provided a direct way to regulate SMC phenotype and thus inhibited the in-stent restenosis. The distinctive loading process of miR-22 and the abandonment of transfection agents highlighted the promising potentials.

Since the acute inflammation usually occurs at the early stage of

Fig. 5. Co-culture evaluation of EC and SMC. (a) Fluorescence micrographs of co-culture cells on different samples. (red: EC, green: SMC); (b) The cell density of EC and SMC, respectively. (n = 5, ***p < 0.001).

Fig. 6. The *in vivo* implantation evaluation of PCEC@miR-22 coated stent. (a) Illustration of the *in vivo* evaluation. The insert confocal micrograph of the stent indicated the uniform distribution of miR-22 on the stent. (b) Masson staining and HE staining tests of the arteries with BSs, MESs, respectively. Histological analysis of neointimal thickness (c), and the percentage of neointimal stenosis (d) (n = 3, *P < 0.05).

repairing [3,26,62], we evaluated the protein expression level that related to the regeneration process after implantation for one week. As shown in Fig. 8a&b, the relative expression of IL-6, an important type of inflammation-associated protein [40,63], was significantly reduced in MESs groups as compared to the BSs. The expression of MCP-1 showed similar trends, indicating relatively low acute inflammation responses in miR-22 eluting stents [64]. Previous studies have revealed that miR-22 could perform a protective and anti-inflammatory effect in myocardial ischemia-reperfusion injury [65,66]. The miR-22 loaded stents in this work showed anti-inflammatory results, indicating a protective regulation of the repairing process. Moreover, the miR-22 target mRNA level of EVI-1 showed a significant downregulation, indicating the efficient miR-22 delivery via the PCEC coating (Fig. S9, supporting information).

We also observed the down-regulative trend of EVI-1 and the significant downregulation of Col-I, suggesting that the delivery of miR-22 was effective to depress the SMC proliferation.

4. Conclusion

In summary, we have realized the effective incorporation of hydrophilic miR-22 via the self-healing encapsulation process of an amphipathic PCL-PEG-PCL (PCEC) triblock copolymer spongy coating for the regulation of the SMC phenotype and suppression of intimal hyperplasia. The PCEC spongy coating realized the uniform and controllable loading of miR-22 to the highest loading dosage of 133.1 pmol cm^{-2} and performed a sustained release behavior in a diffusion-controlled
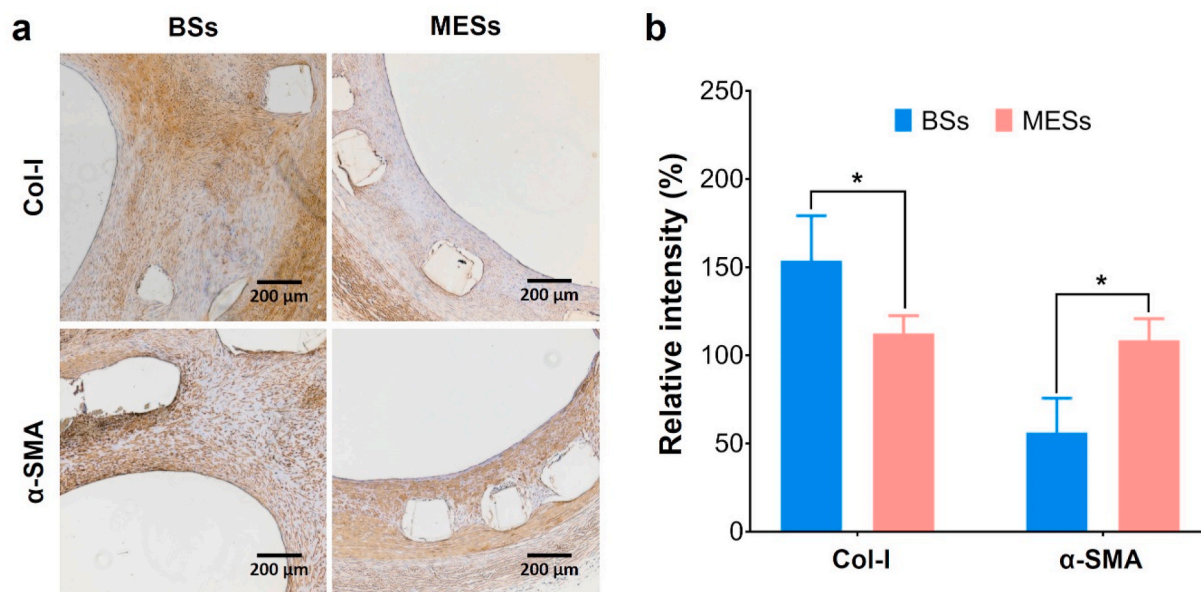
Fig. 7. Immunohistochemical analysis of the stented arterial segments for Col-I and α-SMA (a) and the corresponding relative intensity (b), respectively. (n = 3, *p < 0.05).
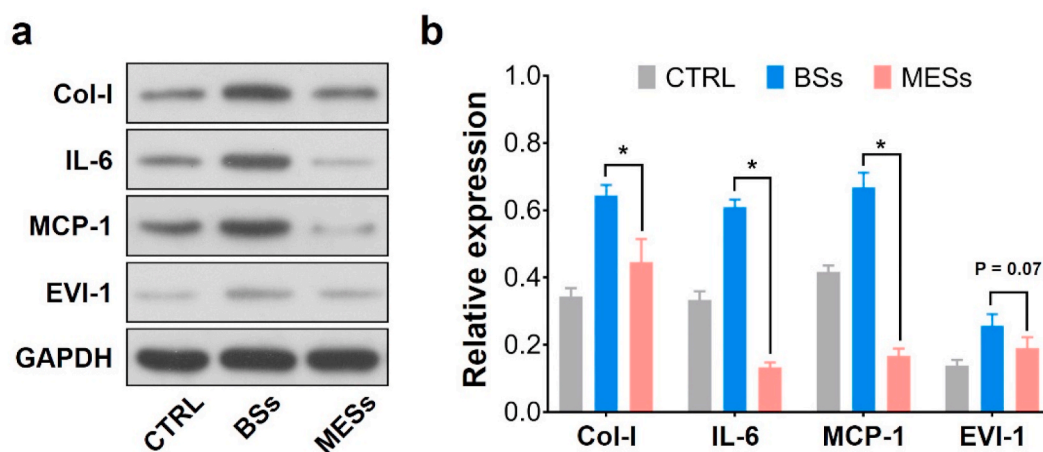
Fig. 8. (a)Western blot analysis of arterial segments implanted with BSs and MESs, respectively. Ctrl represents the native arterial segments. (b) Quantification of Western Blot bands. Values normalized to GAPDH and then normalized to Ctrl. (n = 3, *P < 0.05).

manner. We demonstrated that the surface-mediated delivery of miR-22 at a dosage of 84.2 pmol cm^{-2} dramatically enhanced the contractile phenotype and suppressed the proliferation of SMCs without impairing the proliferation and function of ECs. This selective inhibition effect of PCEC@miR-22 coating contributed to the dominating growth behavior of ECs with an EC/SMC ratio of 5.4 in co-culture evaluation. More importantly, the PCEC@miR-22 stent coating showed reduced inflammation, improved SMC contractile phenotype, and low ECM secretion, which eventually contributed to the inhibition of in-stent restenosis. This work provides a reliable coating platform for the combination of microRNAs with real-life medical devices, which may facilitate new biofunctional materials for clinical applications.

CRediT authorship contribution statement

Jing Wang: designed the research, performed the experiments, Formal analysis, wrote the manuscript. **Hong-Lin Qian:** performed the experiments. **Wei-Pin Huang:** performed SEM data. **Ke-Feng Ren:** designed the research, Formal analysis, supervised the project and

revised the manuscript. **Yun-Bing Wang:** Formal analysis, supervised the project and revised the manuscript. **Guo-sheng Fu:** Formal analysis, supervised the project and revised the manuscript. **Jian Ji:** Formal analysis, supervised the project and revised the manuscript, All authors substantially contributed to the research and reviewed the manuscript.

Declaration of competing interest

The authors declare no conflicts of interest regarding the publication of this paper.

Acknowledgments

Universities (2020FZZX003-01-03), and the Higher Education Discipline Innovation Project (111 Project) under Grant No. B16042.

Appendix A. Supplementary data

Supplementary data to this article can be found online at https://doi.org/10.1016/j.bioactmat.2021.04.037.

References

[1] E.K. Oikonomou, C. Antoniades, The role of adipose tissue in cardiovascular health and disease, Nat. Rev. Cardiol. 16 (2) (2019) 83–99.

[2] D. Zhao, J. Liu, M. Wang, X.G. Zhang, M.G. Zhou, Epidemiology of cardiovascular disease in China: current features and implications, Nat. Rev. Cardiol. 16 (4) (2019) 203–212.

[3] T.F. Luscher, J. Steffel, F.R. Eberli, M. Joner, G. Nakazawa, F.C. Tanner, R. Virmani, Drug-eluting stent and coronary thrombosis - biological mechanisms and clinical implications, Circulation 115 (8) (2007) 1051–1058.

[4] G.G. Stefanini, D.R. Holmes, Drug-eluting coronary-artery stents, N. Engl. J. Med. 368 (3) (2013) 254–265.

[5] D. Bian, L. Qin, W. Lin, D. Shen, H. Qi, X. Shi, G. Zhang, H. Liu, H. Yang, J. Wang, D. Zhang, Y. Zheng, Magnetic resonance (MR) safety and compatibility of a novel iron bioresorbable scaffold, Bioact. Mater. 5 (2) (2020) 260–274.

[6] G.D. Dangas, B.E. Claessen, A. Caixeta, E.A. Sanidas, G.S. Mintz, R. Mehran, In-stent restenosis in the drug-eluting stent era, J. Am. Coll. Cardiol. 56 (23) (2010) 1897–1907.

[7] A.W. Carpenter, M.H. Schoenfisch, Nitric oxide release: part II. Therapeutic applications, Chem. Soc. Rev. 41 (10) (2012) 3742–3752.

[8] Q. Lin, X. Ding, F. Qiu, X. Song, G. Fu, J. Ji, In situ endothelialization of intravascular stents coated with an anti-CD34 antibody functionalized heparin–collagen multilayer, Biomaterials 31 (14) (2010) 4017–4025.

[9] Y. Wei, Y. Ji, L.-L. Xiao, Q.-k. Lin, J.-p. Xu, K.-f. Ren, J. Ji, Surface engineering of cardiovascular stent with endothelial cell selectivity for in vivo re-endothelialisation, Biomaterials 34 (11) (2013) 2588–2599.

[10] B. Lu, X. Han, A. Zhao, D. Luo, M.F. Maitz, H. Wang, P. Yang, N. Huang, Intelligent H2S release coating for regulating vascular remodeling, Bioact. Mater. 6 (4) (2021) 1040–1050.

[11] Y. Li, J. Yan, W. Zhou, P. Xiong, P. Wang, W. Yuan, Y. Zheng, Y. Cheng, In vitro degradation and biocompatibility evaluation of typical biodegradable metals (Mg/Zn/Fe) for the application of tracheobronchial stenosis, Bioact. Mater. 4 (2019) 114–119.

[12] M. Taniwaki, M.D. Radu, S. Zaugg, N. Amabile, H.M. Garcia-Garcia, K. Yamaji, E. Jorgensen, H. Kelbaek, T. Pilgrim, C. Caussin, T. Zanchin, A. Veugeois, U. Abildgaard, P. Juni, S. Cook, K.C. Koskinas, S. Windecker, L. Raber, Mechanisms of very late drug-eluting stent thrombosis assessed by optical coherence tomography, Circulation 133 (7) (2016) 650–660.

[13] T. Adriaenssens, M. Joner, T.C. Godschalk, N. Malik, F. Alfonso, E. Xhepa, D. De Cock, K. Komukai, T. Tada, J. Cuesta, V. Sirbu, L.J. Feldman, F.J. Neumann, A. H. Goodall, T. Heestermans, I. Buysschaert, O. Hlinomaz, A. Belmans, W. Desmet, J.M. ten Berg, A.H. Gershlick, S. Massberg, A. Kastrati, G. Guagliumi, R.A. Byrne, P. l.S. T I, Optical coherence tomography findings in patients with coronary stent thrombosis A report of the PRESTIGE consortium (prevention of late stent thrombosis by an interdisciplinary global European effort), Circulation 136 (11) (2017) 1007–1021.

[14] D.H. Walter, M. Cejna, L. Diaz-Sandoval, S. Willis, L. Kirkwood, P.W. Stratford, A. B. Tietz, R. Kirchmair, M. Silver, C. Curry, A. Wecker, Y.S. Yoon, R. Heidenreich, A. Hanley, M. Kearney, F.O. Tio, P. Kuenzler, J.M. Isner, D.W. Losordo, Local gene transfer of phVEGF-2 plasmid by gene-eluting stents - an alternative strategy for inhibition of restenosis, Circulation 110 (1) (2004) 36–45.

[15] J. Aoki, A.T.L. Ong, E.P. McFaden, W.J. van der Giessen, G. Sianos, E. Regar, P. de Feyter, M.J.B. Kutryk, P.W. Serruys, Endothelial progenitor cell capture by stents coated with antibody against CD34 the HEALING-FIM (healthy endothelial accelerated lining inhibits neointimal growth-first in man) registry, J. Am. Coll. Cardiol. 45 (3) (2005) 69a, 69a.

[16] I. Andreou, P.H. Stone, In-stent atherosclerosis at a crossroads, Circulation 134 (19) (2016) 1413–1415.

[17] J. Wang, Y.F. Xue, J. Liu, M. Hu, H. Zhang, K.F. Ren, Y.B. Wang, J. Ji, Hierarchical capillary coating to biofunctionlize drug-eluting stent for improving endothelium regeneration, Research 2020 (2020) 1458090.

[18] Y. Yang, P. Gao, J. Wang, Q. Tu, L. Bai, K. Xiong, H. Qiu, X. Zhao, M.F. Maitz, H. Wang, X. Li, Q. Zhao, Y. Xiao, N. Huang, Z. Yang, Endothelium-mimicking multifunctional coating modified cardiovascular stents via a stepwise metal-catechol-(amine) surface engineering strategy, Research 2020 (2020) 1–20.

[19] N. Lyu, Z. Du, H. Qiu, P. Gao, Q. Yao, K. Xiong, Q. Tu, X. Li, B. Chen, M. Wang, G. Pan, N. Huang, Z. Yang, Mimicking the nitric oxide-releasing and glycocalyx functions of endothelium on vascular stent surfaces, Adv. Sci. 7 (21) (2020) 2002330.

[20] C.C. Pritchard, H.H. Cheng, M. Tewari, MicroRNA profiling: approaches and considerations, Nat. Rev. Genet. 13 (5) (2012) 358–369.

[21] C. Gareri, S. De Rosa, C. Indolfi, MicroRNAs for restenosis and thrombosis after vascular injury, Circ. Res. 118 (7) (2016) 1170–1184.

[22] T. Barwari, A. Joshi, M. Mayr, MicroRNAs in cardiovascular disease, J. Am. Coll. Cardiol. 68 (23) (2016) 2577–2584.

[23] M.W. Feinberg, K.J. Moore, MicroRNA regulation of atherosclerosis, Circ. Res. 118 (4) (2016) 703–720.

[24] K.R. Cordes, N.T. Sheehy, M.P. White, E.C. Berry, S.U. Morton, A.N. Muth, T. H. Lee, J.M. Miano, K.N. Ivey, D. Srivastava, miR-145 and miR-143 regulate smooth muscle cell fate and plasticity, Nature 460 (7256) (2009) 705. U80.

[25] D. Wang, T. Deuse, M. Stubbendorff, E. Chernogubova, R.G. Erben, S.M. Eken, H. Jin, Y.H. Li, A. Busch, C.H. Heeger, B. Behnisch, H. Reichenspurner, R. C. Robbins, J.M. Spin, P.S. Tsao, S. Schrepfer, L. Maegdefessel, Local MicroRNA modulation using a novel anti-miR21-eluting stent effectively prevents experimental in-stent restenosis, Arterioscl. Throm. Vas. 35 (9) (2015) 1945–1953.

[26] C. Chaabane, F. Otsuka, R. Virmani, M.L. Bochaton-Piallat, Biological responses in stented arteries, Cardiovasc. Res. 99 (2) (2013) 353–363.

[27] K. Yahagi, F.D. Kolodgie, F. Otsuka, A.V. Finn, H.R. Davis, M. Joner, R. Virmani, Pathophysiology of native coronary, vein graft, and in-stent atherosclerosis, Nat. Rev. Cardiol. 13 (2) (2016) 79–98.

[28] S. Torii, H. Jinnouchi, A. Sakamoto, M. Kutyna, A. Cornelissen, S. Kuntz, L. Guo, H. Mori, E. Harari, K.H. Paek, R. Fernandez, D. Chahal, M.E. Romero, F. D. Kolodgie, A. Gupta, R. Virmani, A.V. Finn, Drug-eluting coronary stents: insights from preclinical and pathology studies, Nat. Rev. Cardiol. 17 (1) (2019) 37–51.

[29] X.C. Chen, K.F. Ren, J.H. Zhang, D.D. Li, E. Zhao, Z.J. Zhao, Z.K. Xu, J. Ji, Humidity-triggered self-healing of microporous polyelectrolyte multilayer coatings for hydrophobic drug delivery, Adv. Funct. Mater. 25 (48) (2015) 7470–7477.

[30] X.C. Chen, K.F. Ren, W.X. Lei, J.H. Zhang, M.C.L. Martins, M.A. Barbosa, J. Ji, Self-healing spongy coating for drug "cocktail" delivery, ACS Appl. Mater. Interfaces 8 (7) (2016) 4309–4313.

[31] W.X. Lei, X.C. Chen, M. Hu, H. Chang, H. Xu, K.F. Ren, J. Ji, Dynamic spongy films to immobilize hydrophobic antimicrobial peptides for self-healing bactericidal coating, J. Mater. Chem. B 4 (38) (2016) 6358–6365.

[32] Q.P. Qian, X.P. Huang, X.Y. Zhang, Z.G. Xie, Y.P. Wang, One-step preparation of macroporous polymer particles with multiple interconnected chambers: a candidate for trapping biomacromolecules, Angew. Chem. Int. Ed. 52 (40) (2013) 10625–10629.

[33] R.B. Shah, S.P. Schwendeman, A biomimetic approach to active self-microencapsulation of proteins in PLGA, J. Contr. Release 196 (2014) 60–70.

[34] J. Wang, X.C. Chen, Y.F. Xue, M. Hu, Y.B. Wang, K.F. Ren, J. Ji, Thermo-triggered ultrafast self-healing of microporous coating for on-demand encapsulation of biomacromolecules, Biomaterials 192 (2019) 15–25.

[35] J. Wang, K.-F. Ren, Y.-F. Gao, H. Zhang, W.-P. Huang, H.-L. Qian, Z.-K. Xu, J. Ji, Photothermal spongy film for enhanced surface-mediated transfection to primary cells, ACS Appl. Bio Mater. 2 (6) (2019) 2676–2684.

[36] F. Yang, Q.S. Chen, S.P. He, M. Yang, E.M. Maguire, W.W. An, T.A. Afzal, L. A. Luong, L. Zhang, Q.Z. Xiao, miR-22 is a novel mediator of vascular smooth muscle cell phenotypic modulation and neointima formation, Circulation 137 (17) (2018) 1824–1841.

[37] D. Loessner, C. Meinert, E. Kaemmerer, L.C. Martine, K. Yue, P.A. Levett, T.J. Klein, F.P. Melchels, A. Khademhosseini, D.W. Hutmacher, Functionalization, preparation and use of cell-laden gelatin methacryloyl-based hydrogels as modular tissue culture platforms, Nat. Protoc. 11 (4) (2016) 727–746.

[38] J. Wang, Y.F. Xue, X.C. Chen, M. Hu, K.F. Ren, J. Ji, Humidity-triggered relaxation of polyelectrolyte complexes as a robust approach to generate extracellular matrix biomimetic films, Adv. Healthc. Mater. (2020), e2000381.

[39] M. Hu, H. Chang, H. Zhang, J. Wang, W.X. Lei, B.C. Li, K.F. Ren, J. Ji, Mechanical adaptability of the MMP-responsive film improves the functionality of endothelial cell monolayer, Adv. Healthc. Mater. 6 (14) (2017) 1601410.

[40] H. Zhang, K.F. Ren, H. Chang, J.L. Wang, J. Ji, Surface-mediated transfection of a pDNA vector encoding short hairpin RNA to downregulate TGF-beta 1 expression for the prevention of in-stent restenosis, Biomaterials 116 (2017) 95–105.

[41] X.C. Chen, W.P. Huang, M. Hu, K.F. Ren, J. Ji, Controlling structural transformation of polyelectrolyte films for spatially encapsulating functional species, Small 15 (9) (2019) 1804867.

[42] J. Huang, J.M. Mazzara, S.P. Schwendeman, M.D. Thouless, Self-healing of pores in PLGAs, J. Contr. Release 206 (2015) 20–29.

[43] F.S. Collins, H. Varmus, A new initiative on precision medicine, N. Engl. J. Med. 372 (9) (2015) 793–795.

[44] J.L. Jameson, D.L. Longo, Precision medicine - personalized, problematic, and promising, N. Engl. J. Med. 372 (23) (2015) 2229–2234.

[45] I. Fishbein, I. Alferiev, M. Bakay, S.J. Stachelek, P. Sobolewski, M.Z. Lai, H. Choi, I. W. Chen, R.J. Levy, Local delivery of gene vectors from bare-metal stents by use of a biodegradable synthetic complex inhibits in-stent restenosis in rat carotid arteries, Circulation 117 (16) (2008) 2096–2103.

[46] H. Chang, K.-f. Ren, J.-l. Wang, H. Zhang, B.-l. Wang, S.-m. Zheng, Y.-y. Zhou, J. Ji, Surface-mediated functional gene delivery: an effective strategy for enhancing competitiveness of endothelial cells over smooth muscle cells, Biomaterials 34 (13) (2013) 3345–3354.

[47] M.Y. Adeel, F. Sharif, Advances in stent-mediated gene delivery, Expet Opin. Drug Deliv. 13 (4) (2016) 465–468.

[48] R.L. Du, Y.Z. Wang, Y.H. Huang, Y.P. Zhao, D.C. Zhang, D.Y. Du, Y. Zhang, Z.G. Li, S. McGinty, G. Pontrelli, T.Y. Yin, G.X. Wang, Design and testing of hydrophobic core/hydrophilic shell nano/micro particles for drug-eluting stent coating, NPG Asia Mater. 10 (2018) 642–658.

[49] S.K. Gupta, A. Foinquinos, S. Thum, J. Remke, K. Zimmer, C. Bauters, P. de Groote, R.A. Boon, L.J. de Windt, S. Preissl, L. Hein, S. Batkai, F. Pinet, T. Thum, Preclinical development of a MicroRNA-based therapy for elderly patients with myocardial infarction, J. Am. Coll. Cardiol. 68 (14) (2016) 1557–1571.

[50] P. Gurha, C. Abreu-Goodger, T.N. Wang, M.O. Ramirez, A.L. Drumond, S. van Dongen, Y.Q. Chen, N. Bartonicek, A.J. Enright, B. Lee, R.J. Kelm, A.K. Reddy, G.

E. Taffet, A. Bradley, X.H. Wehrens, M.L. Entman, A. Rodriguez, Targeted deletion of MicroRNA-22 promotes stress-induced cardiac dilation and contractile dysfunction, Circulation 125 (22) (2012) 2751. U209.

[51] B. Tian, X. Ding, Y. Song, W. Chen, J. Liang, L. Yang, Y. Fan, S. Li, Y. Zhou, Matrix stiffness regulates SMC functions via TGF-beta signaling pathway, Biomaterials 221 (2019) 119407.

[52] X.K. Ren, Y.K. Feng, J.T. Guo, H.X. Wang, Q. Li, J. Yang, X.F. Hao, J. Lv, N. Ma, W. Z. Li, Surface modification and endothelialization of biomaterials as potential scaffolds for vascular tissue engineering applications, Chem. Soc. Rev. 44 (15) (2015) 5680–5742.

[53] K.H. Bonaa, J. Mannsverk, R. Wiseth, L. Aaberge, Y. Myreng, O. Nygard, D. W. Nilsen, N.E. Klow, M. Uchto, T. Trovik, B. Bendz, S. Stavnes, R. Bjornerheim, A. I. Larsen, M. Slette, T. Steigen, O.J. Jakobsen, O. Bleie, E. Fossum, T.A. Hanssen, O. Dahl-Eriksen, I. Njolstad, K. Rasmussen, T. Wilsgaard, J.E. Nordrehaug, N. Investigators, Drug-eluting or bare-metal stents for coronary artery disease, N. Engl. J. Med. 375 (13) (2016) 1242–1252.

[54] G.L. Basatemur, H.F. Jorgensen, M.C.H. Clarke, M.R. Bennett, Z. Mallat, Vascular smooth muscle cells in atherosclerosis, Nat. Rev. Cardiol. 16 (12) (2019) 727–744.

[55] E.D. Michos, J.W. McEvoy, R.S. Blumenthal, Lipid management for the prevention of atherosclerotic cardiovascular disease, N. Engl. J. Med. 381 (16) (2019) 1557–1567.

[56] S. Yang, J. Graham, J.W. Kahn, E.A. Schwartz, M.E. Gerritsen, Functional roles for PECAM-1 (CD31) and VE-cadherin (CD144) in tube assembly and lumen formation in three-dimensional collagen gels, Am. J. Pathol. 155 (3) (1999) 887–895.

[57] G.I. Mun, I.S. Kim, B.H. Lee, Y.C. Boo, Endothelial argininosuccinate synthetase 1 regulates nitric oxide production and monocyte adhesion under static and laminar shear stress conditions, J. Biol. Chem. 286 (4) (2011) 2536–2542.

[58] F. Otsuka, A.V. Finn, S.K. Yazdani, M. Nakano, F.D. Kolodgie, R. Virmani, The importance of the endothelium in atherothrombosis and coronary stenting, Nat. Rev. Cardiol. 9 (8) (2012) 439–453.

[59] H. Chang, X.Q. Liu, M. Hu, H. Zhang, B.C. Li, K.F. Ren, T. Boudou, C. Albiges-Rizo, C. Picart, J. Ji, Substrate stiffness combined with hepatocyte growth factor modulates endothelial cell behavior, Biomacromolecules 17 (9) (2016) 2767–2776.

[60] S.A. Xie, T. Zhang, J. Wang, F. Zhao, Y.P. Zhang, W.J. Yao, S.S. Hur, Y.T. Yeh, W. Pang, L.S. Zheng, Y.B. Fan, W. Kong, X. Wang, J.J. Chiu, J. Zhou, Matrix stiffness determines the phenotype of vascular smooth muscle cell in vitro and in vivo: role of DNA methyltransferase 1, Biomaterials 155 (2018) 203–216.

[61] Y. Zhao, G. Zang, T. Yin, X. Ma, L. Zhou, L. Wu, R. Daniel, Y. Wang, J. Qiu, G. Wang, A novel mechanism of inhibiting in-stent restenosis with arsenic trioxide drug-eluting stent: enhancing contractile phenotype of vascular smooth muscle cells via YAP pathway, Bioact. Mater. 6 (2) (2021) 375–385.

[62] M. Back, A. Yurdagul Jr., I. Tabas, K. Oorni, P.T. Kovanen, Inflammation and its resolution in atherosclerosis: mediators and therapeutic opportunities, Nat. Rev. Cardiol. 16 (7) (2019) 389–406.

[63] L. Chung, D.R. Maestas Jr., F. Housseau, J.H. Elisseeff, Key players in the immune response to biomaterial scaffolds for regenerative medicine, Adv. Drug Deliv. Rev. 114 (2017) 184–192.

[64] T.J. Guzik, D.S. Skiba, R.M. Touyz, D.G. Harrison, The role of infiltrating immune cells in dysfunctional adipose tissue, Cardiovasc. Res. 113 (9) (2017) 1009–1023.

[65] J. Yang, L.H. Chen, J.W. Ding, J. Zhang, Z.X. Fan, C.J. Yang, Q.Q. Yu, J. Yang, Cardioprotective effect of miRNA-22 on hypoxia/reoxygenation induced cardiomyocyte injury in neonatal rats, Gene 579 (1) (2016) 17–22.

[66] J. Yang, Z.X. Fan, J. Yang, J.W. Ding, C.J. Yang, L.H. Chen, microRNA-22 attenuates myocardial ischemia-reperfusion injury via an anti-inflammatory mechanism in rats, Exp. Ther. Med. 12 (5) (2016) 3249–3255.